

Improving the accuracy of the neuroevolution machine learning potential for multi-component systems

Zheyong Fan^{1,*}

¹College of Physical Science and Technology, Bohai University, Jinzhou 121013, P. R. China
(Dated: September 24, 2021)

In a previous paper [Fan Z *et al.* 2021 Phys. Rev. B, **104**, 104309], we developed the neuroevolution potential (NEP), a framework of training neural network based machine-learning potentials using a natural evolution strategy and performing molecular dynamics (MD) simulations using the trained potentials. The atom-environment descriptor in NEP was constructed based on a set of radial and angular functions. For multi-component systems, all the radial functions between two atoms are multiplied by some fixed factors that depend on the types of the two atoms only. In this paper, we introduce an improved descriptor for multi-component systems, in which different radial functions are multiplied by different factors that are also optimized during the training process, and show that it can significantly improve the regression accuracy without increasing the computational cost in MD simulations.

I. INTRODUCTION

In recent years, machine-learning (ML) potentials [1–5] have played an important role in molecular dynamics (MD) simulations. A well trained ML potential can achieve an accuracy close to that of the training data and a speed that cannot be achieved by *ab initio* MD simulations. After the pioneering work by Behler and Parrinello [6] on the high-dimensional neural network (NN) potential, other alternatives such as the Gaussian approximation potential (GAP) [7] and some linear regression ML potentials [8, 9] were also developed. State-of-the-art NN potentials such as the deep potential (DP) [10] have been developed by exploring standard ML libraries.

Recently, the present author developed a framework called neuroevolution potential (NEP) [11] for training NN-based ML potential using a natural evolution strategy [12, 13], instead of the conventional back propagation (gradient descent) approach. NEP has been implemented in version 2.6 of the open-source GPUMD package [14, 15]. It has been demonstrated [11] that NEP as implemented in GPUMD can achieve an accuracy comparable to other popular implementations of ML potentials [16–18], while exhibiting a much higher computational efficiency in MD simulations.

In this paper, we show that for multi-component systems, i.e., systems with multiple atom types, the accuracy of NEP can be significantly improved. We present the improved approach and implement it version 2.7 of GPUMD. For simplicity, the NEPs as implemented in versions 2.6 and 2.7 of GPUMD will be called NEP1 and NEP2, respectively. We will use bulk PbTe as a case study to show the improved accuracy of NEP2 as compared to NEP1.

II. THEORY

A. The previous NEP1

The ML potential in NEP1 [11] is a local many-body one, where “local” means that the total potential energy U of a system of N atoms can be written as a sum of site energies:

$$U = \sum_{i=1}^N U_i. \quad (1)$$

The site energy U_i of atom i is taken as a function of a set of N_{des} descriptor components $\{q_{\nu}^i\}_{\nu=1}^{N_{\text{des}}}$:

$$U_i = U_i \left(\{q_{\nu}^i\}_{\nu=1}^{N_{\text{des}}} \right), \quad (2)$$

which is a many-variable scalar function.

NEP1 uses a NN with a single hidden layer with N_{neu} neurons, the state of which can be represented as a vector, x_{μ} ($1 \leq \mu \leq N_{\text{neu}}$). The hidden layer state vector is obtained from the input descriptor vector by a combination of linear and nonlinear transforms:

$$x_{\mu} = \tanh \left(\sum_{\nu=1}^{N_{\text{des}}} w_{\mu\nu}^{(1)} q_{\nu}^i - b_{\mu}^{(1)} \right), \quad (3)$$

where $w_{\mu\nu}^{(1)}$ is the connection weight between the neurons x_{μ} and q_{ν}^i , and $b_{\mu}^{(1)}$ is the bias for the neuron x_{μ} . The hyperbolic tangent function is chosen as the nonlinear activation function in the hidden layer. Then, the site energy is taken as the output layer state, which is calculated as a linear combination of the state vector of the hidden layer:

$$U_i = \sum_{\mu=1}^{N_{\text{neu}}} w_{\mu}^{(2)} x_{\mu} - b^{(2)}, \quad (4)$$

where $w_{\mu}^{(2)}$ is the connection weight between the neurons U_i and x_{μ} , and $b^{(2)}$ is the bias for the neuron U_i .

* brucenju@gmail.com

For a central atom i , there is a set of radial descriptor components ($0 \leq n \leq n_{\max}^R$),

$$q_n^i = \sum_{j \neq i} g_n(r_{ij}), \quad (5)$$

and a set of angular descriptor components ($0 \leq n \leq n_{\max}^A$ and $1 \leq l \leq l_{\max}$),

$$q_{nl}^i = \sum_{j \neq i} \sum_{k \neq i} g_n(r_{ij}) g_n(r_{ik}) P_l(\cos \theta_{ijk}), \quad (6)$$

where $P_l(\cos \theta_{ijk})$ is the Legendre polynomial of order l , θ_{ijk} being the angle formed by the ij and ik bonds. The functions $g_n(r_{ij})$ are radial functions and they are defined as

$$g_n(r_{ij}) = \frac{T_n \left(2 \left(\frac{r_{ij}}{r_c} - 1 \right)^2 - 1 \right) + 1}{2} f_c(r_{ij}) c_{ij}. \quad (7)$$

Here $T_n(x)$ is the n -th order Chebyshev polynomial of the first kind and $f_c(r_{ij})$ is the cutoff function defined as

$$f_c(r_{ij}) = \frac{1}{2} \left(1 + \cos \left(\pi \frac{r_{ij}}{r_c} \right) \right) \quad (8)$$

for $r \leq r_c$ and $f_c(r_{ij}) = 0$ for $r > r_c$. The cutoff radius r_c can take different values for the radial and angular components, which are denoted as r_c^R and r_c^A , respectively.

Following Refs. 19 and 20, a factor c_{ij} is included in the definition of the radial functions $g_n(r_{ij})$ to account for the different atom types. Gastegger *et al.* [19] suggested to use $c_{ij} = z_j$, where z_j is the atomic number of atom j and Artrith *et al.* [20] suggested to use $c_{ij} = \pm 1, \pm 2, \dots$. In NEP1, c_{ij} is chosen as $\sqrt{z_i z_j}$.

B. The improved NEP2

It is clear that in all the schemes above, the resulting descriptor has the permutation symmetry, i.e., the descriptor is invariant upon a permutation of the atoms with the same type. However, hand-chosen values for c_{ij} might not be optimal. More importantly, the coefficients c_{ij} are the same for all the radial functions $g_n(r_{ij})$, which do not depend on n . In NEP2, we propose to make these coefficients n -dependent, leading to the following radial functions:

$$g_n(r_{ij}) = \frac{T_n \left(2 \left(\frac{r_{ij}}{r_c} - 1 \right)^2 - 1 \right) + 1}{2} f_c(r_{ij}) c_{nij}. \quad (9)$$

If the considered material has N_{typ} atom types, the number of c_{nij} coefficients is

$$N_{\text{typ}}^2 (n_{\max}^R + n_{\max}^A + 2). \quad (10)$$

For example, when $N_{\text{typ}} = 2$, $n_{\max}^R = 12$, and $n_{\max}^A = 6$, there will be 80 c_{nij} parameters. These c_{nij} parameters

are not hand chosen, but are taken as free parameters to be optimized during the training process, similar to the weight and bias parameters in the NN. One difference between the c_{nij} parameters and the NN parameters is that we require that

$$|c_{nij}| \geq \frac{1}{10}. \quad (11)$$

The purpose of applying this restriction is to avoid too small values for the descriptor components.

We stress that the introduction of more parameters to the radial functions does not add more computations to the ML potential, as the number of descriptor components and the number of NN parameters, which affect the speed of the potential in MD simulations, are not changed. With this in mind, we next evaluate the regression accuracy of NEP2 as compared to NEP1.

III. RESULTS AND DISCUSSION

We use the training data set of bulk PbTe as studied in Ref. 11 to compare NEP1 and NEP2. The training data set is publicly available in Zenodo [21]. All the hyperparameters in the descriptor are the same for NEP1 and NEP2: $r_c^R = 8 \text{ \AA}$, $r_c^A = 4 \text{ \AA}$, $n_{\max}^R = 12$, $n_{\max}^A = 6$, $l_{\max} = 4$, and $N_{\text{neu}} = 40$. The population size in the natural evolution strategy is 50 and the \mathcal{L}_1 and \mathcal{L}_2 regularization weights defined in Ref. 11 are both 0.05.

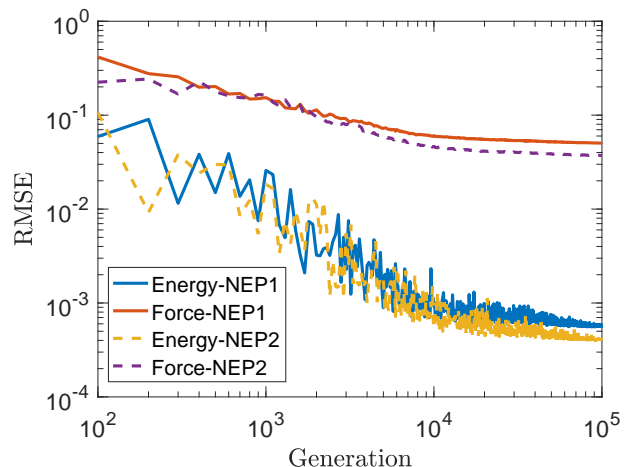


FIG. 1. Evolution of the energy and force RMSEs during the training process for NEP1 (solid lines) and NEP2 (dashed lines).

Figure 1 shows the evolution of the root mean square errors (RMSEs) of energy and force as obtained by NEP1 and NEP2 with respect to the generation in the natural evolution strategy. The total number of generations is chosen as 10^5 here, which is large enough to achieve convergence of the RMSEs. Within the first few thousand

generations, the RMSEs are comparable between NEP1 and NEP2. However, NEP2 develops smaller RMSEs afterwards. Up to 10^5 generations, the energy and force RMSEs obtained in NEP1 are 0.56 meV/atom and 50 meV/Å respectively. The corresponding values obtained in NEP2 are 0.40 meV/atom and 37 meV/Å. The reduction of regression errors is about 30% for both energy and force. We stress that this enhancement of regression accuracy is achieved without affecting the computational speed in MD simulations using the trained potentials.

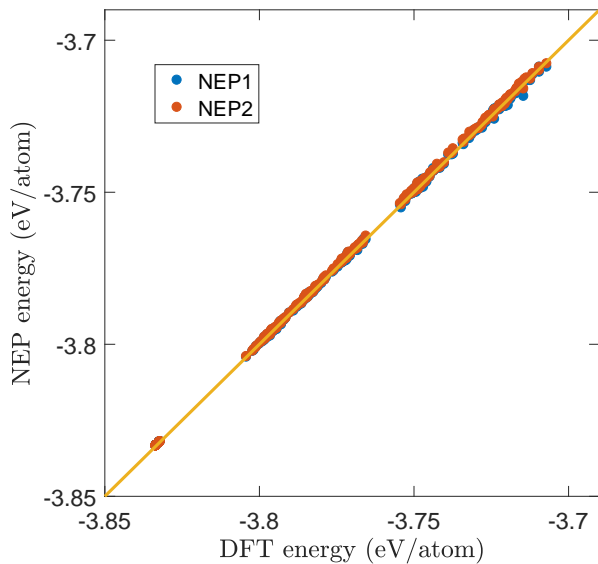


FIG. 2. Energy as calculated from NEP1 and NEP2 compared with the training data from quantum mechanical DFT calculations. The solid line represents the identity function used to guide the eyes.

Figure 2 compares the predicted energies by NEP1 and NEP2 and those from quantum mechanical density functional theory (DFT) calculations. Figure 3 shows similar results for force. It can be seen that the energy and force errors from NEP2 are indeed smaller than those from NEP1. Particularly, in NEP1, there are some force errors larger than 0.5 eV/Å, which are absent from NEP2.

To better appreciate the performance of NEP2, we compare it with both NEP1 and some other popular ML potential packages [16–18]. Figure 4 shows the force regression accuracy and MD speed for NEP1, NEP2, GAP, moment tensor potential (MTP) [9, 17], and DP. The MD speed is measured as the product of the number of atoms and the number of steps that can be achieved per second. For GAP and MTP, 72 Intel Xeon-Gold 6240 CPU cores are used; for DP and NEP (both NEP1 and NEP2), one Nvidia Tesla V100 GPU is used. These CPU and GPU resources are of comparable price. We see that NEP2 can achieve a high accuracy and a high computational speed simultaneously.

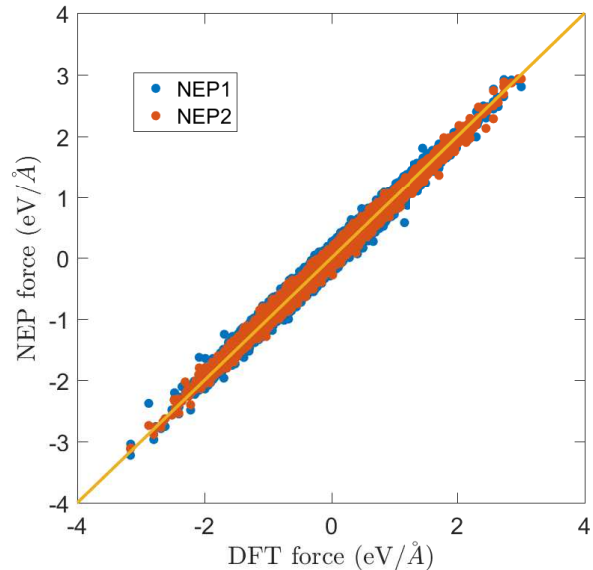


FIG. 3. Force as calculated from NEP1 and NEP2 compared with the training data from quantum mechanical DFT calculations. The solid line represents the identity function used to guide the eyes.

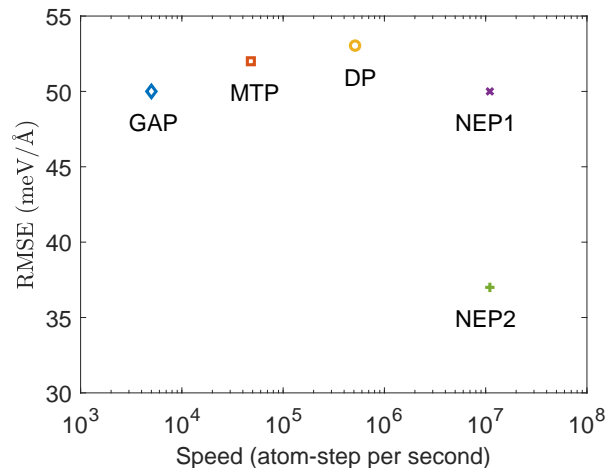


FIG. 4. Force RMSE and MD speed for the various ML potentials trained using the same set of training data for PbTe. The results for NEP1, GAP, MTP and DP are taken from Ref. 11.

To understand the origin of the higher accuracy achievable by NEP2 compared to NEP1, we examine the distributions of some descriptor components in Fig. 5. Here we consider the radial descriptor component q_n with $n = 4$ and the angular descriptor component q_{nl} with $n = 5$ and $l = 4$ for the Pb and Te atoms in the whole training data set. In NEP1, the distributions of q_4 for Pb and Te have some overlap, while those of q_{54} for Pb and

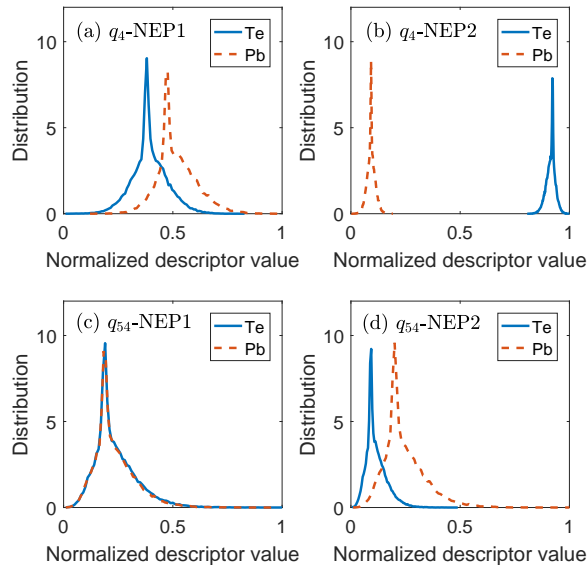


FIG. 5. Distribution of the normalized q_4 and q_{54} descriptor components for NEP1 and NEP2. The distributions for the Pb atoms (dashed lines) and Te atoms (solid lines) are separately considered.

Te are almost identical. In NEP2, the distributions of q_4 for Pb and Te are well separated, while those of q_{54} for Pb and Te have small overlap only. We see that for both components, the distributions for Pb and Te are more distinguishable in NEP2, which can help to better discriminate the two atom types. Similar results exist for other descriptor components as well. Therefore, optimizing the c_{nij} parameters in Eq. (9) for each radial

function can lead to better discrimination of the different atom types in a multi-component system. This is the origin of the higher accuracy of NEP2 compared to NEP1.

IV. SUMMARY AND CONCLUSIONS

In summary, we have proposed an improved scheme of considering different atom types in the atom-environment descriptor used in the neuroevolution machine-learning potential. The improved method leads to higher regression accuracy without increasing the computational cost in molecular dynamics simulations. The improved neuroevolution potential is implemented in version 2.7 of the open-source GPUMD package.

The method can also be applied to neural network potentials trained using the back propagation method, but one needs to compute the derivatives of a loss function with respect to the extra parameters introduced into the descriptor. By contrast, the introduction of these parameters adds little extra work in our approach as the natural evolution strategy does not require the calculation of the derivative of the loss function with respect to any parameter. This is one of the advantages of the natural evolution strategy compared to back propagation.

ACKNOWLEDGMENTS

ZF acknowledges the supports from the National Natural Science Foundation of China (NSFC) (No. 11974059) and the Science Foundation from Education Department of Liaoning Province under Grant No. LQ2019010.

-
- [1] Jörg Behler, “Perspective: Machine learning potentials for atomistic simulations,” *The Journal of Chemical Physics* **145**, 170901 (2016).
 - [2] Volker L. Deringer, Miguel A. Caro, and Gábor Csányi, “Machine learning interatomic potentials as emerging tools for materials science,” *Advanced Materials* **31**, 1902765 (2019).
 - [3] Tim Mueller, Alberto Hernandez, and Chuhong Wang, “Machine learning for interatomic potential models,” *The Journal of Chemical Physics* **152**, 050902 (2020).
 - [4] Y. Mishin, “Machine-learning interatomic potentials for materials science,” *Acta Materialia* **214**, 116980 (2021).
 - [5] Oliver T. Unke, Stefan Chmiela, Huziel E. Sauceda, Michael Gastegger, Igor Poltavsky, Kristof T. Schütt, Alexandre Tkatchenko, and Klaus-Robert Müller, “Machine learning force fields,” *Chemical Reviews* **121**, 10142–10186 (2021).
 - [6] Jörg Behler and Michele Parrinello, “Generalized neural-network representation of high-dimensional potential-energy surfaces,” *Phys. Rev. Lett.* **98**, 146401 (2007).
 - [7] Albert P. Bartók, Mike C. Payne, Risi Kondor, and Gábor Csányi, “Gaussian Approximation Potentials: The Accuracy of Quantum Mechanics, without the Electrons,” *Phys. Rev. Lett.* **104**, 136403 (2010).
 - [8] A.P. Thompson, L.P. Swiler, C.R. Trott, S.M. Foiles, and G.J. Tucker, “Spectral neighbor analysis method for automated generation of quantum-accurate interatomic potentials,” *Journal of Computational Physics* **285**, 316–330 (2015).
 - [9] Alexander V. Shapeev, “Moment tensor potentials: A class of systematically improvable interatomic potentials,” *Multiscale Modeling & Simulation* **14**, 1153–1173 (2016).
 - [10] Linfeng Zhang, Jiequn Han, Han Wang, Roberto Car, and Weinan E, “Deep potential molecular dynamics: A scalable model with the accuracy of quantum mechanics,” *Phys. Rev. Lett.* **120**, 143001 (2018).
 - [11] Zheyong Fan, Zezhu Zeng, Cunzhi Zhang, Yanzhou Wang, Keke Song, Haikuan Dong, Yue Chen, and Tapio Ala-Nissila, “Neuroevolution machine learning po-

- tentials: Combining high accuracy and low cost in atomistic simulations and application to heat transport,” *Phys. Rev. B* **104**, 104309 (2021).
- [12] Tom Schaul, Tobias Glasmachers, and Jürgen Schmidhuber, “High dimensions and heavy tails for natural evolution strategies,” in *Proceedings of the 13th Annual Conference on Genetic and Evolutionary Computation*, GECCO ’11 (Association for Computing Machinery, New York, NY, USA, 2011) pp. 845–852.
- [13] Daan Wierstra, Tom Schaul, Tobias Glasmachers, Yi Sun, Jan Peters, and Jürgen Schmidhuber, “Natural evolution strategies,” *Journal of Machine Learning Research* **15**, 949–980 (2014).
- [14] Zheyong Fan, Topi Siro, and Ari Harju, “Accelerated molecular dynamics force evaluation on graphics processing units for thermal conductivity calculations,” *Computer Physics Communications* **184**, 1414 – 1425 (2013).
- [15] Zheyong Fan, Wei Chen, Ville Vierimaa, and Ari Harju, “Efficient molecular dynamics simulations with many-body potentials on graphics processing units,” *Computer Physics Communications* **218**, 10 – 16 (2017).
- [16] <https://github.com/libAtoms/QUIP>.
- [17] Ivan S Novikov, Konstantin Gubaev, Evgeny V Podryabinkin, and Alexander V Shapeev, “The MLIP package: moment tensor potentials with MPI and active learning,” *Machine Learning: Science and Technology* **2**, 025002 (2021).
- [18] Han Wang, Linfeng Zhang, Jiequn Han, and Weinan E, “DeepPMD-kit: A deep learning package for many-body potential energy representation and molecular dynamics,” *Computer Physics Communications* **228**, 178–184 (2018).
- [19] M. Gastegger, L. Schwiedrzik, M. Bittermann, F. Berzsenyi, and P. Marquetand, “wACSF-Weighted atom-centered symmetry functions as descriptors in machine learning potentials,” *The Journal of Chemical Physics* **148**, 241709 (2018).
- [20] Nongnuch Artrith, Alexander Urban, and Gerbrand Ceder, “Efficient and accurate machine-learning interpolation of atomic energies in compositions with many species,” *Phys. Rev. B* **96**, 014112 (2017).
- [21] Zheyong Fan, “Inputs and outputs of nep in gpumd,” (2021).